Experiments and Modelling towards Long Pulse High Confinement Operation with Radiofrequency Heating and Current Drive in EAST

Y. Peysson[1], X.Z. Gong[2], M. Goniche[1], J.P. Qian[2], L. Colas[1], B.J. Ding[2], A. Ekedahl[1], W. Helou[1], J. Hillairet[1], G.T. Hoang[1], M.H. Li[2], S. Lin[2], F.K. Liu[2], C.M. Qin[2], Y.T. Song[2], L. Valade[1], X.J. Wang[2], X.J. Zhang[2], B. Zhang[2], Y.P. Zhao[2], X.L. Zou[1] and the EAST Team[2]

[1] CEA, IRFM, F-13108 Saint Paul-lez-Durance, France.
[2] Institute of Plasma Physics, Chinese Academy of Sciences, Hefei 230031, P. R. China.

Email: yves.peysson@cea.fr

Abstract. The radiofrequency (RF) heating and current drive systems play a crucial role in the mission of the Experimental Advanced Superconducting Tokamak (EAST). RF experiments and modelling have been carried out on EAST in 2015-2016, with the aim to optimize EAST long pulse scenarios, and at the same time gain experience in view of exploitation of the WEST device. Experiments have been carried out to assess the current drive efficiency of the LHCD systems in different plasma configurations and with different gas feeding. The CD efficiency of the two LHCD systems (2.45 GHz and 4.6 GHz), has been compared and full non-inductive LHCD discharges have been compared to modelling with the C3PO/LUKE codes. In experiments aiming at long pulse H-mode scenarios, H-modes have been sustained by RF heating systems (LHCD, ECRH, ICRH) in both Upper Single Null (W-divertor) and Lower Single Null (carbon divertor) configurations, with loop voltage maintained as low as 50 mV during 6 seconds long pulses.

1. Introduction

The radiofrequency (RF) heating and current drive systems play a crucial role in the mission of the Experimental Advanced Superconducting Tokamak (EAST) and are primordial for reaching long pulse, high-confinement (H-mode) plasmas on EAST [1]. This paper reports on RF experiments and modelling carried out on EAST in 2015-2016, within the framework of the Associated Laboratory ASIPP-IRFM, with the aim to optimize EAST long pulse scenarios, and at the same time gain experience before the exploitation of the WEST device [2]. For example, the unique Lower Hybrid Current Drive (LHCD) capability, i.e. two LHCD systems at different frequencies (4.6 GHz [3] and 2.45 GHz [4]), has allowed comparing the CD efficiency of the two LHCD systems [5]. Extensive modelling with the ray-tracing + Fokker-Planck codes C3PO/LUKE [6] has been performed. Other experiments, mainly focusing on the 4.6 GHz antenna, have been carried out to study the CD efficiency in different plasma configurations (Upper Single Null versus Lower Single Null) and with different gas feeding locations. In view of long pulse H-mode scenarios, a series of H-mode experiments has been conducted where all the heating power was provided by RF heating methods only, i.e. LHCD, ECRH (Electron Cyclotron Resonance Heating) and ICRH (Ion Cyclotron Resonance Heating).

In addition to the experiments and modelling results presented here, EAST experiments have revealed some operational issues important for long pulse operation. During the 2015 campaign, arcing at the 4.6 GHz antenna, accompanied by emission of flakes near the antenna and divertor regions, was observed via visible cameras. Following the in-vessel inspections, several corrective actions were taken before the 2016 campaign: i) new LH antenna guard limiters were installed; ii) the LH antenna mouth was positioned radially closer to the guard limiters in order to reduce the electric field at antenna mouth; iii) all in-vessel components were cleaned from deposits that had accumulated during previous plasma operation. The results from the commissioning phase in early 2016 seemed to indicate improved power handling of the 4.6 GHz antenna, as well as improved plasma performance.

2. LH wave coupling

The effect of particle fueling on the average power reflection coefficient (RC) of the 4.6 GHz antenna was studied using gas injection from different locations, combined with Supersonic Molecular Beam Injection (SMBI). These experiments were carried out in the Upper Single Null (USN) configuration, which has the strike points on the W-divertor. Most of the particles were provided by the standard gas injection and the SMBI was used for the feedback control of the line-averaged density which was ramped from 2.5×10^{19} m^{-3} to 4×10^{19} m^{-3}. For the three different gas injection locations tested (high field side, low field side and upper divertor), the RC is identical in the whole density range (Figure 1). It is noticeable that the RC is almost constant at 6% for quite a large part of the density ramp and then drops to 4% when the density exceeds 3.5×10^{19} m^{-3}. This drop is correlated with the phase of the discharge where the largest amount of particle fueling comes from SMBI, a method that has been found to increase radial transport [7]. This effect is clearly beneficial for increasing the density in the far scrape-off layer and thus beneficial for the LH coupling.
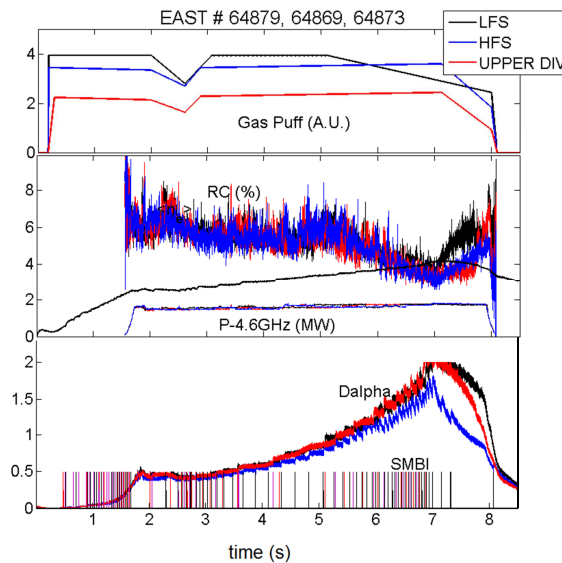

FIG. 1: Average reflection coefficient (RC) of the 4.6 GHz antenna for different gas fueling schemes (B_T = 2.5 T, I_P = 0.5 MA).

3. LHCD efficiency

3.1 LH wave propagation effects

In order to assess the effect of the magnetic configuration on the LH wave propagation, similar discharges with a density ramp were conducted in the USN and the Lower Single Null (LSN) configuration (B_T = 2.5 T, I_P = 0.5 MA, $P_{LH\_4.6GHz}$ = 1.7 MW). The electron cyclotron emission (ECE) from fast electrons driven by the LH wave, which is down-shifted by the relativistic effect and therefore measured at the very periphery of the plasma (R = 2.30 m, r/a = 1), was used as a qualitative measure of the difference in LHCD efficiency. The ECE signal was significantly larger in the USN configuration (around 30% larger) in the whole density range explored, as seen in Figure 2a. The bremsstrahlung from these fast electrons in the hard X-ray range is also enhanced in the USN configuration, and the internal inductance is reduced. The total energy content is also found to be slightly higher (+ 10%) for the USN configuration. In addition, the RF spectrum in the 4.58 - 4.61 GHz range was recorded by a magnetic loop outside the vacuum vessel. Figure 2b shows that when the density exceeds 3×10^{19} m^{-3}, the width of the pump wave (at f = 4.6 GHz) is larger for the LSN configuration. This could suggest that the wave number spectrum is affected by scattering on density fluctuations or by a parametric decay into an ion-sound wave (f ~ 2-3 MHz) [5, 8].
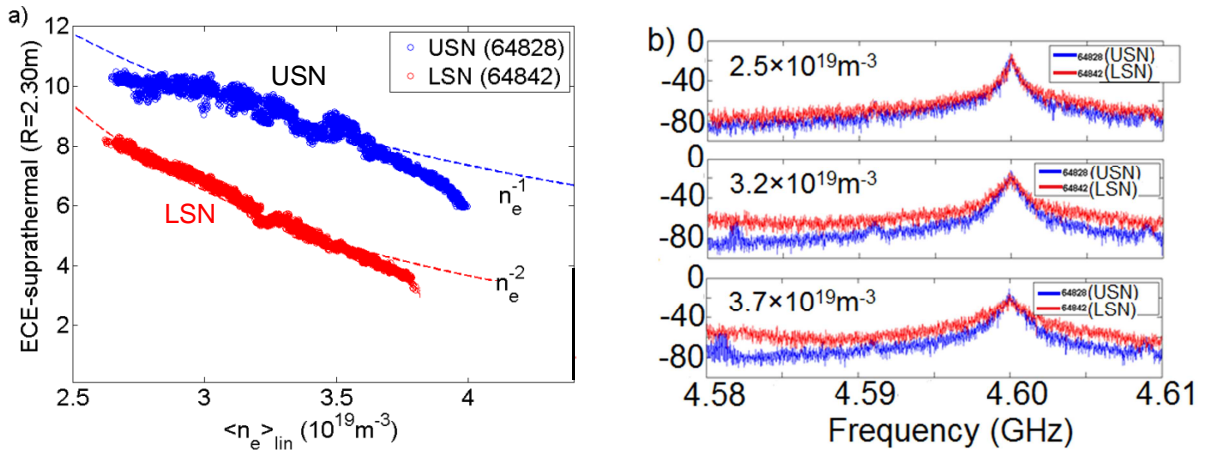

FIG. 2: Non-thermal ECE (a) and RF spectra in dB (b) in the USN (#64828) and LSN (#64842) configurations ($P_{LH\_4.6GHz}$ = 1.7 MW).

In order to quantify the propagation effects and the resulting up-shift of the wave index ($N_{//}$) on the LHCD efficiency, two discharges were performed in the same plasma configuration (identical to discharge #64842) and the same power ($P_{LH\_4.6GHz}$ = 0.4 MW), launched by either the three lower rows of waveguides or the three upper rows. The average reflection coefficient (RC) was very similar for the two discharges in the entire density range (RC ~ 3%), which indicates that the launched $N_{//}$ spectra (whose directivity and thus CD efficiency can be affected by RC [9]) can be considered to be the same. A slight difference on the loop voltage and the total stored energy (W_{MHD}) at the benefit of the top launch is found (Figure 3). When the line-averaged density exceeds 3.4×10^{19} m^{-3}, a strong interaction of the antenna with

the edge plasma occurs, which is also related to an increase of the gas injected by SMBI, and the stored energy decreases.
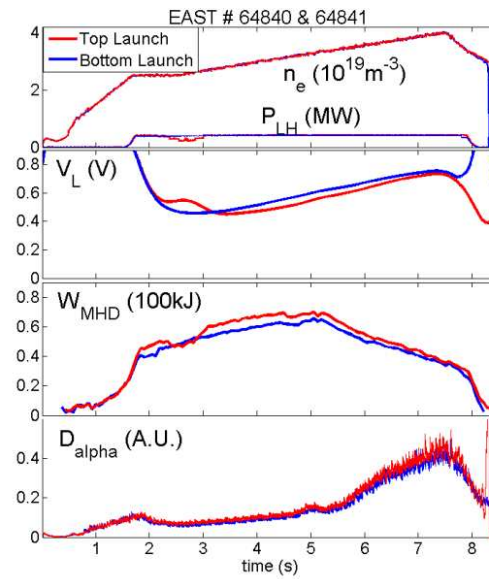

FIG. 3: Effect of the wave launch position (B_T = 2.5 T, I_P = 0.5 MA, LSN configuration). Slightly higher efficiency is deduced for the top launch case.

3.2 Effect of LH antenna frequency

In H-mode operation, both LHCD antennas are used in order to maximize the non-inductive current fraction and thus extend the pulse duration. H-mode discharges have been sustained by LHCD + ICRH (P_{LH} = 1.8-3.2 MW; P_{ICRH} = 1.2-1.5 MW), in which most of the plasma current (I_p = 0.4 MA) is non-inductively driven (loop voltage < 140 mV). At low loop voltage (V_{Loop}), it can be shown that V_{Loop} varies almost linearly with P_{norm}, where P_{norm} = $P_{LH}/(<n_e>_{lin}.R.I_p)$, and that the CD efficiency is given by $1/P_{norm}$ at V_{Loop} = 0 [10]. In the density range of interest, i.e. line averaged density $<n_e>_{lin}$ = 2.4-3.2×10^{19} m^{-3}, the loop voltage decreases linearly with P_{norm}, only if the contribution of the power launched by the 2.45 GHz antenna to P_{LH} is weighted by a factor 0.5. Similar result was inferred from V_{Loop} measurements at modest LH power (~ 1 MW), launched by the two antennas separately in the same discharge [5]. The same weighting also leads to less spread when fitting the hard X-ray data and the total plasma energy. Neglecting the bootstrap current for these low beta discharges, the global efficiency is found to be close to $0.78×10^{19}$ A.W^{-1}m^{-2}. At the limited range of density used in these discharges, no deleterious effect of the density on the LHCD efficiency could be observed.

The result above suggests that a fraction of the power launched from the 2.45 GHz antenna may be damped at the plasma edge and not entering the plasma core. This interpretation is partially consistent with RF spectrum measurements in the scrape-off layer, which indicate broader pump width for the 2.45 GHz antenna [5, 8]. Electron acceleration at the plasma edge due to Landau damping on high $N_{//}$-components does not seem to be the cause, since infrared measurements of the divertor do not indicate higher heat load with the 2.45 GHz antenna. In

addition, calculations of the electron acceleration using the electric field from ALOHA [11] and a model for the electron dynamics in the LH electric field based on [12], show that the heat flux produced by edge electron acceleration is comparable for the two antennas [13].

4. Modelling of LHCD in EAST

First principle quantitative modelling has been carried out for various plasma conditions and LH antenna phasing with the C3PO/LUKE codes [6]. An example of ray trajectories used for current drive simulations for EAST tokamak is shown in Figure 4 using the ray-tracing code C3PO [14]. In the ray-tracing calculations, several rays are launched from the poloidal positions corresponding to each waveguide row (which in the case in Figure 4 is five rows, for the 2.45 GHz antenna).
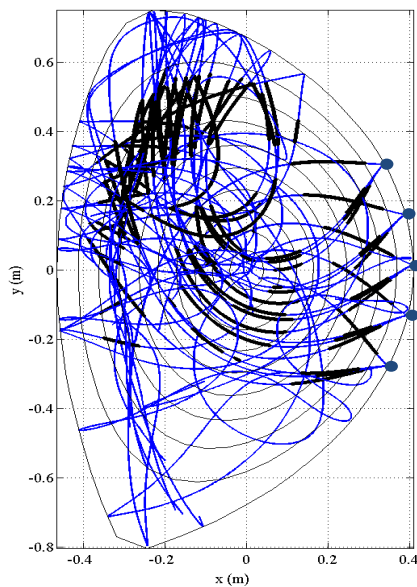

FIG. 4: Rays calculated by C3PO ray-tracing code for an EAST discharge whose toroidal plasma current is fully driven by the LH wave.
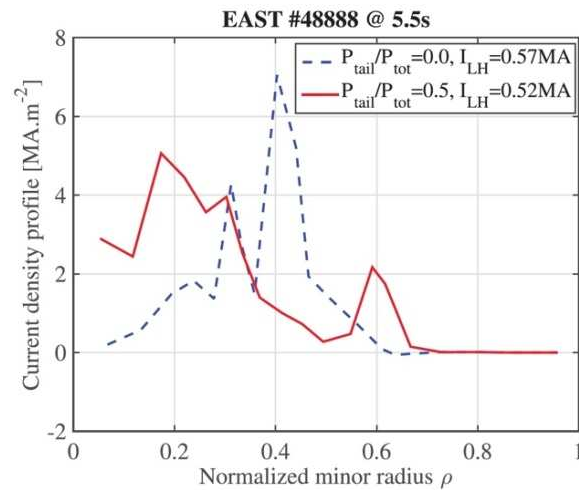
FIG. 5: LH current density profiles from C3PO/LUKE, with fast-fluctuating power spectrum (solid) and without (dashed).

A fully non-inductive diverted discharge at $\langle n_e \rangle_{lin} = 2.5 \times 10^{19}$ m^{-3} and $P_{LH} = 2.25$ MW at 4.6 GHz was found experimentally to produce about 0.39 MA non-inductive current [15]. During LHCD, the core electron temperature reaches 3 keV in the steady-state regime, without evidence of sawtooth activity, and the estimated internal inductance, $l_i = 1.22$, remains unchanged compared to the Ohmic phase, within error bars. The standard ray-tracing and Fokker-Planck calculations with C3PO/LUKE yield off-axis LH current density profile and hollow calculated hard X-ray profile, in disagreement with experimental observations. However, by introducing a fast-fluctuating power spectrum at the plasma edge, leading to a tail in the launched power spectrum at the separatrix carrying 50% of the LH power, the calculated LH current density profile becomes more central and broad, as shown in Figure 5. In this case, the LH current density profile is close to the toroidal MHD equilibrium one, which is consistent with the measured internal inductance and the lack of sawteeth. However,

in order to retrieve lower level of plasma current, consistent with experiments, an anomalous radial transport of the fast electrons proportional to $v_\parallel$ must be introduced in the calculations with a diffusion rate of $D_{\psi\psi0} = 0.4 \ m^2 s^{-1}$ from $v_\parallel = v_{th}$.

Extended studies of various EAST discharges at zero loop voltage have confirmed the importance of the tail in the initial LH power spectrum for ray-tracing calculations. By adding a tail in the initial power spectrum, consistent results can be simultaneously obtained with measured line-integrated hard X-ray profiles between 20-200 keV, the toroidal plasma current and the internal inductance. Indeed, without considering a tail, in particular the predicted internal inductance is well below the experimentally observed values, thus highlighting that the LH power absorption is likely rather central. The anomalous transport alone cannot contribute to shift the LH power absorption towards the plasma core, while keeping the current at the experimental level.

The impact of the LH wave frequency on the current drive efficiency has been investigated with C3PO/LUKE. With the given input parameters, the ray-tracing + Fokker-Planck calculations cannot reproduce the experimental results, i.e. a higher CD efficiency for the 4.6 GHz system compared to the 2.45 GHz system [5]. The power spectra for the two LH antennas, used as input to C3PO, were calculated with ALOHA [11] coupling code for the antenna phasing used in the experiments. A refined analysis is necessary to identify if the difference in efficiency may result from slight changes of the antenna directivity, as found in Tore Supra [9], not yet been considered in the modelling, or if this effect is the signature of an extrinsic process that is not yet considered in the present simulations.

5. H-mode experiments

A study of the H-mode access with RF heating systems only was carried out on EAST in 2016, in a plasma configuration as close as possible to that foreseen in WEST [2]. The maximum available heating power in the particular experiment was limited to ~ 3.6 MW (P_{LHCD} ~ 2.8 MW, P_{ICRH} ~ 0.4 MW, P_{ECRH} ~ 0.4 MW). Nevertheless, H-mode plasmas lasting 6 seconds, close to zero loop voltage (V_{Loop} ~ 50mV) could be achieved. One example is shown in Figure 6. The plasma configuration in the discharge in Figure 6 (#64971) was LSN, i.e. with the strike point on the carbon divertor, and with $B \times \nabla B$ directed towards the target, which is expected to be favourable for the transition to H-mode [16]. The L-H transition occurred very early, at 2.2 s, after the application of 2.5 MW LHCD (see Figure 6). ECRH power was applied slightly later, at 2.6 s. In these experiments, it was found that low power ECRH and/or ICRH could be beneficial for sustaining the H-mode throughout the pulse. When changing the toroidal magnetic field direction so that $B \times \nabla B$ was directed away from the target, while keeping the plasma configuration and density the same, no H-mode transition was obtained even though the total injected power was increased to 3.6 MW.

The same set of experiments was later repeated in the Upper Single Null (USN) configuration, i.e. with the strike points on the W-divertor. One discharge with $B\times\nabla B$ directed upwards towards the W-divertor, which again is expected to be favourable for the L-H transition, is shown in Figure 7. The H-mode is again sustained throughout the duration of the heating phase, at higher density and with comparable H-factor, as in Figure 6. When reversing the $B\times\nabla B$ direction in USN configuration, while maintaining the same heating power as in #65072 from LHCD, ICRH and ECRH, only a short lasting H-mode (~ 1 s) was obtained, that transited back to L-mode, even though the heating power remained constant.
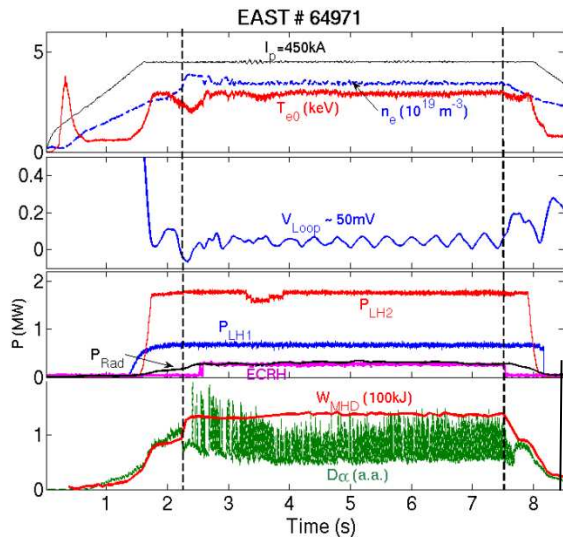

FIG. 6: Time traces of H-mode discharge in LSN configuration, B_T = -2.5T and $B\times\nabla B$ directed downwards, towards the target (H_{98y} ~ 0.76).
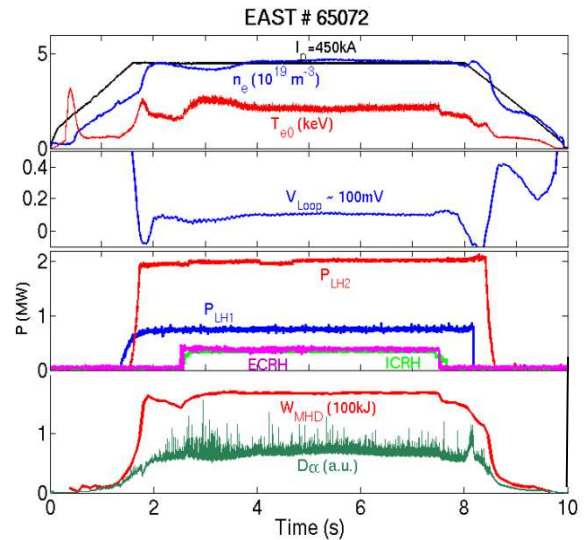
FIG. 7: H-mode discharge in USN configuration (W-divertor), B_T = 2.5T and $B\times\nabla B$ directed upwards, towards the target (H_{98y} ~ 0.78).

In the discharges studied in this set of experiment (I_P = 0.45 MA, B_T = ±2.5 T), high density (n_e ~3×10^{19} m^{-3}) was required in most discharges to trigger the H-mode. Nevertheless, H-modes were also obtained with LHCD alone at low power (P_{LH2} ~ 1.6MW), low density (n_e = 2.5×10^{19} m^{-3}) and high H-factor (H_{98y} ~ 1.1), using the USN configuration and $B\times\nabla B$ directed upwards. However, these discharges transit back to L-mode after approximately 2 s.

6. Summary

Several experiments have been carried out on EAST with the goal to optimizing the efficiency of the RF systems (so far mainly the LHCD systems), in view of long pulse H-mode operation. The LHCD experiments indicate that the USN configuration could be more favourable than the LSN for the current drive efficiency. The different gas feeding location tested (high field side, low field side and upper divertor) do not affect the LH wave coupling differently. However, gas fueling with SMB has shown to reduce the reflection coefficient, due the increase of density in the scrape-off layer, linked to increased radial transport during SMBI. The LHCD experiments are accompanied by modelling using C3PO/LUKE. Extended studies of various zero loop voltage discharges have confirmed the

importance of the tail in the initial LH power spectrum for ray-tracing calculations. By adding a tail in the initial power spectrum, consistent results can be simultaneously obtained with measured line-integrated hard X-ray profiles between 20-200 keV, toroidal plasma current and internal inductance.

During H-mode experiments, 6 seconds long H-modes were obtained with loop voltage as low as 50 mV, using LHCD as main heating and current drive source, accompanied by low power ECRH and/or ICRH. Easier access to H-mode was indeed found when the B×∇B drift was directed towards the target. This was confirmed in both LSN (carbon divertor) and USN (W-divertor) configurations. In summary, all results obtained here also give valuable information in view of the exploitation of the WEST tokamak, which has similar size to EAST, and which will use RF heating methods only in W-environment.

Acknowledgments

References

[1] WAN, B., et al., Nucl. Fusion **55** (2015) 104015.
[2] BOURDELLE, C., et al., Nucl. Fusion **55** (2015) 063017.
[3] LIU, F.K., et al., Nucl. Fusion **55** (2015) 123022.
[4] KONG, E.H., et al., Plasma Phys. Control. Fusion **56** (2014) 075016.
[5] LI. M.H., et al., submitted to Phys. Plasmas (2016).
[6] PEYSSON, Y., and DECKER, J., Fusion Sci. Technol. **65** (2014) 22.
[7] ZOU, X.L., et al., Proc. 24th Int. Conf. on Fusion Energy 2012 (San Diego, CA, 2012), [PD/P8-08].
[8] DING, B.J., et al., this conference.
[9] NILSSON, E., et al., Nucl. Fusion **53** (2013) 083018.
[10] GONICHE, M., et al., Phys. Plasmas **21** (2014) 061515.
[11] HILLAIRET, J., et al., Nucl. Fusion **50** (2010) 125010.
[12] FUCHS, V., et al., Nucl. Fusion **43** (2003) 341.
[13] VALADE, L., AIP Conf. Proc. **1689** (2015) 080007.
[14] PEYSSON, Y., et al., Plasma Phys. Control. Fusion **54** (2012) 045003.
[15] PEYSSON, Y., et al., Plasma Phys. Control. Fusion **58** (2016) 044008.
[16] MCKEE, G.R., et al., Nucl. Fusion **49** (2009) 115016.